Upper limits on the mixing of heavy neutrinos in the beta decay of ^{63}Ni

D. W. Hetherington,* R. L. Graham, M. A. Lone, J. S. Geiger, and G. E. Lee-Whiting
Atomic Energy of Canada Limited Research Company, Chalk River Nuclear Laboratories, Chalk River, Ontario, Canada K0J 1J0
(Received 17 March 1987)

The beta spectrum of ^{63}Ni was studied with a $\pi\sqrt{2}$ beta spectrometer, a multistrip source, and multidetector array. No evidence was found for heavy neutrinos with masses ranging from 4 to 40 keV. The upper limit, including numerical evaluation of systematic errors, for the mixing of a 17 keV neutrino was set at 0.3% (90% confidence level). The beta spectrum endpoint was found to be 66.946±0.020 keV, about 1 keV higher than the value derived from the 1983 atomic mass table, 65.92±0.15 keV.

I. INTRODUCTION

In recent reports, Simpson[1,2] has interpreted a distortion at the low energy end of the tritium beta spectrum as evidence for a 3% mixing of a neutrino of mass 17 keV with the usual light neutrino associated with beta decay. If true, this conclusion would have profound consequences in the fields of elementary particles and cosmology,[3] and the same effect should appear in all other beta spectra.

Several recent measurements on the beta spectrum of ^{35}S (Refs. 4–8) have not supported the existence of the 17 keV neutrino. On the one hand, the conclusions of some of these have been disputed;[2,9] on the other hand, the distortions in Simpson's data have been interpreted by others as the result of instrumental effects or of an incorrect assessment of energy balance or screening corrections.[10–13]

Simpson drew our attention to the fact that a measurement of the shape of the ^{63}Ni beta spectrum could provide an ideal test of the existence of the 17 keV neutrino. This spectrum's endpoint (67 keV) is lower than that of ^{35}S, offering better resolution and counting statistics, but high enough to avoid the very low energy problems associated with tritium. It has a single allowed branch with a half-life long enough (100 yr) to avoid normalization problems.

One other group[14] has measured the ^{63}Ni beta spectrum and found no evidence to support heavy neutrino mixing. Our preliminary data on ^{63}Ni presented at the 1986 Osaka Conference[15] also showed no evidence for the 17 keV neutrino. However, there was some concern about this conclusion because of the presence of relatively strong absorption in the detector window (440 μg/cm^2 aluminum coated Mylar) and other possible instrumental effects. In this paper we present results from an entirely new set of data taken with a thinner window and with explicit evaluation of the impact of instrumental corrections.

II. APPARATUS AND DATA ACQUISITION

A. Spectrometer

The experiment was performed with the Chalk River iron-free $\pi\sqrt{2}$ beta spectrometer[16] (Fig. 1). An array of 22 proportional counters[17] was installed to enhance the data collection counting rate. The counters had entrance slits 1.6 mm wide by 10 cm high, were spaced 1 cm apart, and were filled with isobutane at 20 kPa (150 Torr) pressure. A single entrance window ($\approx$168 μg cm^{-2}) consisting of two layers of polypropylene coated in cellulose nitrate, chromium and gold[18] was used. The detector plane was tilted at 42° to the spectrometer radius. This angle, coupled with a source angle of 20°, optimized the spectrometer resolution while keeping it constant across the detector plane. Extra antiscatter baffles were added to the spectrometer after preliminary measurements showed an excess of counts above the endpoint of the ^{63}Ni spectrum.

B. Source

To enhance the count rate without sacrificing resolution, a large area multiple strip source with appropriate biasing potentials[19] was constructed (Fig. 2). Each strip was 4 mm wide, 10 cm high, and curved (1 m radius) to minimize the effect of spectrometer aberrations. Conducting strips of aluminum (10 μg/cm^2) were evaporated onto a thick masked Plexiglas backing and onto this was evaporated the ^{63}Ni. The total source strength was about 2 mCi and the average surface density of the nickel layer was about 2.5 μg/cm^2. The average energy loss for 50 keV electrons due to source thickness was estimated to be about 5 eV. For calibration purposes, a source of ^{169}Yb was made in identical form. The surface density of this source was estimated to be comparable to or less than that of the ^{63}Ni source.

C. Instrumentation

Pulses from the counters were amplified and then processed by 22 single channel analyzers set to function only as lower level discriminators (Fig. 2). A multi-input scaler interfaced to a Nuclear Data 6660 computer registered and stored the counts in a 22 spectrum array. The average dead time of each counter channel was 7 μs, which was negligible at the low count rates ($<$100 cps) encountered in this experiment.

The data acquisition time for each spectrometer field setting was controlled by an external timer interfaced to the computer. The timer was gated by a count inhibit

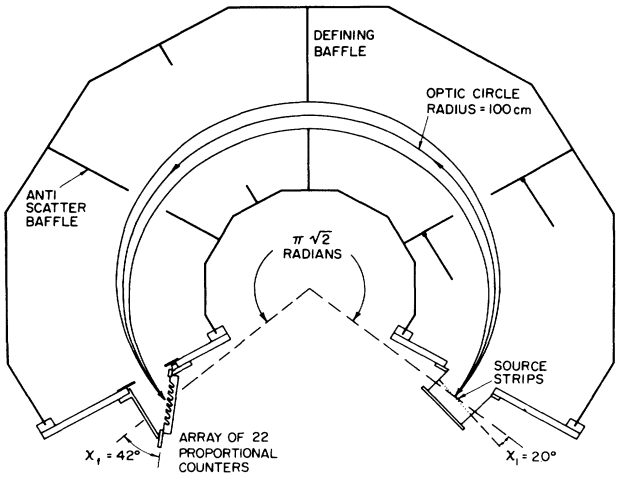

FIG. 1. Plan section through the vacuum chamber of the Chalk River iron-free $\pi\sqrt{2}$ beta spectrometer (Ref. 16) after modifications described in the text.

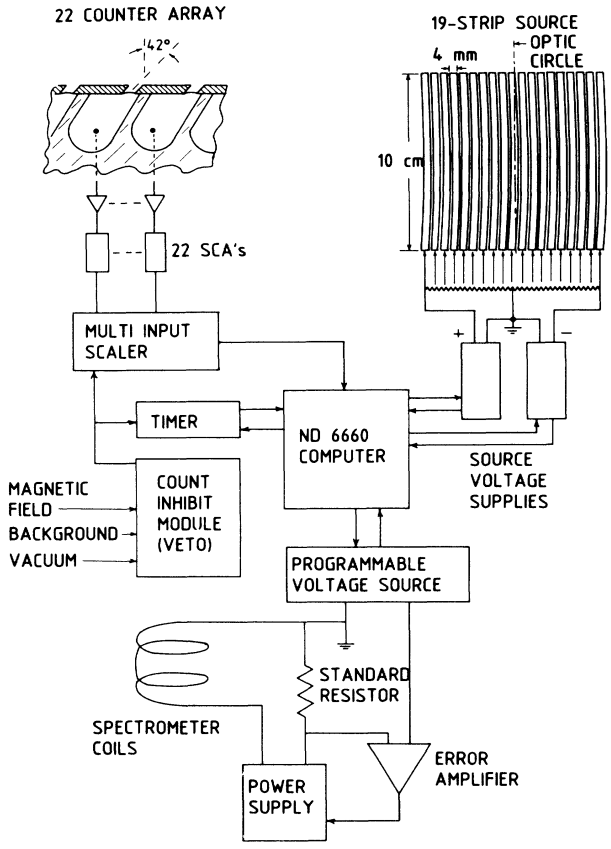

FIG. 2. Schematic representation showing the role of the computer in setting the spectrometer field and source strip voltages and in collecting data from the proportional counters.

(veto) module which suspended data acquisition when any of its input signals (spectrometer vacuum, external magnetic field, and background) were outside prescribed limits. Background, which was monitored with a NaI detector, came mainly from cosmic rays and ^{41}Ar vented from a nearby reactor. The latter caused the background to fluctuate widely at times.

The spectrometer magnetic field was also controlled by the ND 6660 computer via a programmable reference voltage source as shown in Fig. 2. The voltage drop across a standard resistor passing the spectrometer coil current was held equal to the reference voltage by appropriate feedback current control circuitry. The system was accurate and stable to one part in 10^5.

The required bias potential for the off-axis strips of the source, predicted by a second order formula, were established by measurement for the range of electron energies studied in the ^{63}Ni experiments. The central source strip was grounded; two high voltage power supplies and a resistive voltage divider chain provided the correct bias to the other strips within ± 2 V. The output of the power supplies was adjusted by the computer for each magnetic field setting of the spectrometer.

D. Data acquisition

Data from the ^{63}Ni source were obtained over the energy range 25–70 keV in 900 equal momentum steps (about 60 eV per step at 50 keV). Several runs were done for a total acquisition time of 18.7 min in each channel (step) of each of the 22 spectra. In each run, the magnetic field was scanned up through the prescribed range and back down to the initial value. The total electron count accumulated in these scans was $\approx 8\times 10^7$. Additional scans were done in the energy range 46–54 keV for an additional acquisition time of 15 min per channel per spectrum and an additional electron count of $\approx 10^7$. On several occassions, the ^{63}Ni source was replaced with the ^{169}Yb source for calibration and resolution checks. Data were obtained on the ^{169}Yb conversion electron lines with the same step size as for ^{63}Ni as well as with finer steps to obtain detailed line shape and intensity information.

During all data acquisition the entrance slits of three detectors at each end of the array were covered with an aluminum plate. Data from these were used to correct for the cosmic ray and fluctuating ^{41}Ar background.

III. DATA CORRECTION AND CONSOLIDATION

To facilitate analysis, a single consolidated spectrum, incorporating known instrumental corrections, was constructed from the 22 raw spectra, one from the data of each detector, in the following sequence:

(1) background was subtracted from each spectrum;

(2) each spectrum was corrected for detector relative efficiency;

(3) all spectra were shifted to a common calibration and added together;

(4) the consolidated spectrum was corrected for the dependence of resolution on momentum.

A. Background subtraction

The background from external sources varied with time but was independent of the spectrometer momentum setting. Thus counts in a given channel of the six background monitors provided a good measure of the background contribution to the counts in the same channel of the other 16 spectra. After correction for the relative sensitivities of all detectors to background [Fig. 3(c)], the average number of counts in the background monitors was subtracted from each of the other 16 spectra according to Eq. (1).

$$N'_{k,i}=N_{k,i}-\frac{b_k}{6}\sum_j\left[\frac{N_{j,i}}{b_j}\right], \tag{1}$$

where $N_{k,i}$ is the number of counts for detector k in channel i of each of the 16 spectra, b_k is the relative sensitivity of detector k to background, and $j=1,2,3,20,21,22$ denotes the background monitors. The variance (σ^2) for each data point was also calculated.

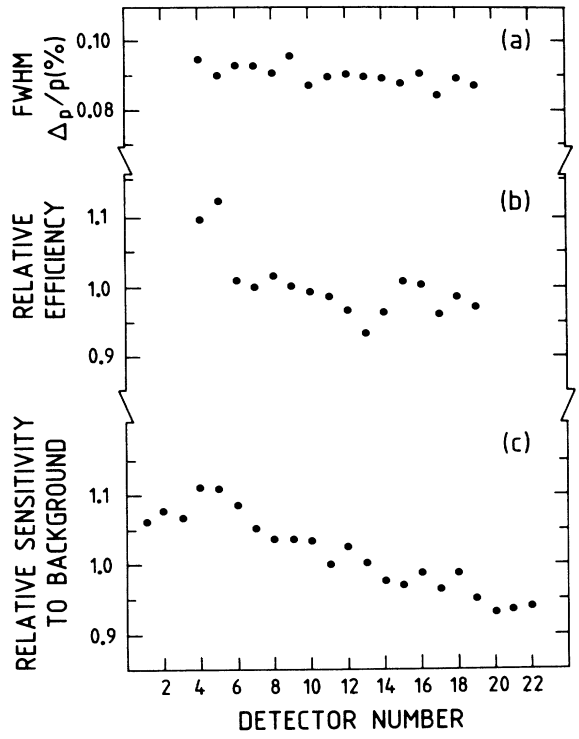

FIG. 3. Properties relating to the 22-element array of proportional counters: (a) The upper section shows the momentum resolution (full width at half maximum) for active detectors 4–19. The first three and last three were blanked off to serve as background monitors. (b) Relative efficiency for all active detectors based on the areas of the 34, 50, and 71 keV conversion electron lines of ^{169}Yb. The differences are due mainly to variations in the widths of the entrance slits. Corresponding variations are not seen in (a); the resolution is determined primarily by the 4 mm width of the source strips. (c) Relative sensitivity to background for all detectors. The trend across the array is caused by differences in the shielding geometry; the inner detector (no. 1) has less Pb shielding than the outermost detector (no. 22).

$$(\sigma^2_{k,i})'=N_{k,i}+\left[\frac{b_k}{6}\right]^2\sum_j\left[\frac{N_{j,i}}{b_j^2}\right]. \tag{2}$$

B. Detector efficiency correction

One factor that affected the efficiency of each detector was the lower level discriminator setting. The discriminators were set as low as possible to minimize this effect and the number of counts lost below the threshold was evaluated from the pulse height spectrum as shown in Fig. 4. Count losses calculated from the difference between the ungated spectrum (Fig. 4, curve *B*) and the gated spectrum (Fig. 4, curve *A*), were constant with electron energy at about 0.9% as shown in Fig. 4(c). On the assumption that the observed drop in counts in the ungated spectrum below channel 6 [Fig. 4(b)] might be due to discriminator losses in the ADC, count losses were also estimated from a constant extrapolation of the pulse height spectrum to channel zero as shown by curve *C*, Fig. 4(b). This calculation produced losses decreasing linearly with energy by about 0.7% over the range of energies scanned in the ^{63}Ni spectrum as shown by curve *C* in Fig. 4(c). Most of the analyses reported here were based on the constant loss assumption (*B*). If curve *C* is valid, then there is a change of $\approx$0.7% over the energy range of interest; this would have some slight effect on

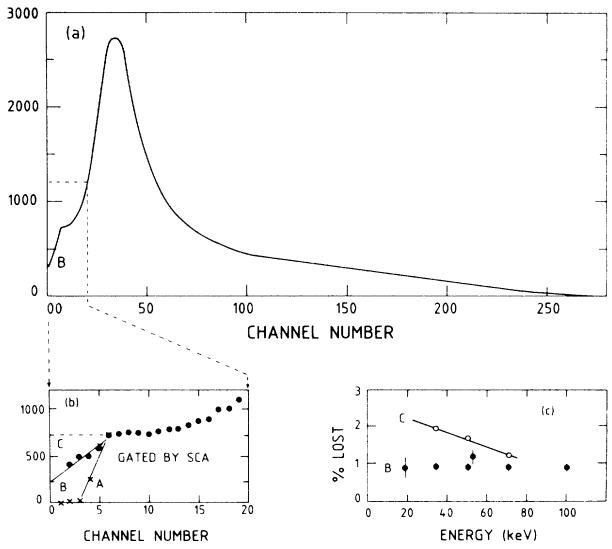

FIG. 4. Deduction of count losses due to electronics: (a) An ungated pulse height spectrum from one of the proportional counters for 50 keV electrons. (b) Lower part of the pulse-height spectrum. The dots are the ungated spectrum; crosses are the spectrum gated by the SCA in lower level discriminator mode. A pulser was used to ensure that channel zero corresponded to zero pulse height. Noise in channel 1 was rejected by the analog-to-digital convertor discriminator. (c) Estimate of lost counts as a function of electron energy. The closed circles (*B*) indicate the area between ungated [*B* in (b)] and gated (*A*) pulse height spectra. The open circles indicate the losses in the constant extrapolation hypothesis (*C*).

the shape parameter, α, discussed in Sec. IV A but not on other parameters.

Tests were made to measure the influence of electric fields produced by the source strip biasing on the properties of the spectrometer. First the relevant Yb internal conversion electron lines were measured with a single-strip source; then the measurements were repeated using a 19-strip ^{169}Yb source with appropriate bias voltages. A small shift in calibration was observed when the source voltages were turned on. To determine the effect on spectrometer transmission (solid angle) the areas of strong conversion lines in a spectrum from the biased multistrip source were compared with the same areas in a spectrum from the single-strip unbiased source. Within an uncertainty of about 0.5%, the relative areas of the peaks in the spectra from the two sources were found to be the same over the range of energies of interest; therefore, no correction was required for the effects of electrostatic biasing. These areas were also used to measure the relative efficiencies of the 16 active detectors; they were found to be independent of electron energy confirming that the effects discussed in the preceding paragraphs, even if not negligible, at least affected all detectors in the same way. The efficiency correction applied in the data consolidation process [Fig. 3(b)] was based on the areas of the conversion electron lines (34, 50, and 71 keV) in the ^{169}Yb spectrum. The variance of the number of counts in each channel of each spectrum was adjusted to reflect the efficiency correction. The effects of detector window transmission, which are not included in this correction, were included in the response function (Sec. IV C).

C. Data consolidation

Since the resolution of the different detectors was very nearly constant across the detector array [Fig. 3(a)], the 16 individual spectra could be added together without loss of information. The calibration for each spectrum, based on the ^{169}Yb peaks, depended on the position of the corresponding detector in the spectrometer focal plane. All spectra were therefore shifted to a common calibration before being added together. This was accomplished by integrating the number of counts in the original spectrum over the momentum "bins" defined by the new calibration. Only that part of the spectrum that was scanned by all detectors was included. The common momentum bins used for the wide scan data were equivalent to five steps in the original data and those for the narrow scan data were equivalent to two steps. The same process was used to calculate the variance of each point in the consolidated spectrum.

D. Resolution correction

In a magnetic spectrometer, the resolution (Δp) is proportional to the momentum of the electrons being counted ($\Delta p/p = \text{const}$). For a continuous beta spectrum, this has the effect of increasing the count rate in proportion to momentum. To correct for this, the number of counts in each channel of the consolidated spectrum was multiplied by a factor of p_0/p ($p_0 = 230$ keV/c). The variances were accordingly multiplied by a factor of $(p_0/p)^2$. Kurie plots of the upper portion of the consolidated wide scan data and of the entire narrow scan consolidated spectrum are shown in Fig. 5.

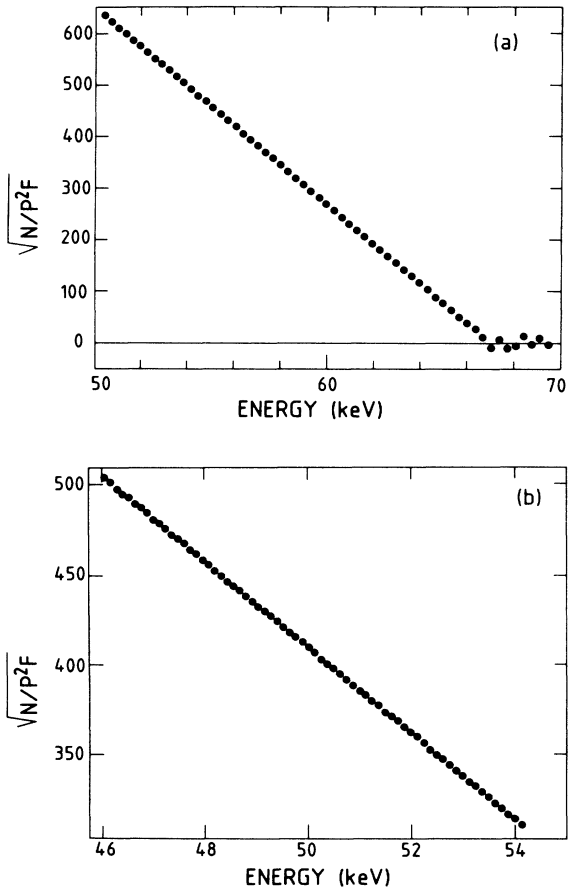

FIG. 5. (a) Kurie plot of the upper part of the consolidated wide scan spectrum. (b) Kurie plot of all of the consolidated narrow scan spectrum.

Data from ^{169}Yb were processed by the same consolidation procedure to check for errors. The conversion electron peaks show no significant distortion or loss of resolution.

IV. DATA ANALYSIS PROCEDURE

A. Parameters

For an electron antineutrino that is a mixture of two mass eigenstates,

$$|\nu_e\rangle = U_{e1}|\nu_1\rangle + U_{e2}|\nu_2\rangle \ , \tag{3}$$

the distribution of electrons in a beta spectrum is given by

$$\frac{dI}{dp} = KSFp^2\{(1-|U_{e2}|^2)(E_0-E)^2 + |U_{e2}|^2(E_0-E)[(E_0-E)^2-m_2^2]^{1/2}\}+B, \tag{4}$$

where K is a constant, S is the shape factor (or correction), F is the Fermi function with screening corrections,[20] p is the electron momentum, E is the electron kinetic energy, E_0 is the extrapolated spectrum endpoint energy, m_2 is the heavy neutrino mass (m_1 is assumed to be zero), and B is the residual background.

Due to its critical effect on the few channels near the endpoint, any background left after the subtraction procedure described in Sec. III must be accounted for in the analysis. The value of this residual background, B, assumed to be constant, was set equal to the average number of counts in the first 20 channels above the endpoint [channel spacing that of Fig. 5(a)]. Changing the value of B by one standard deviation had no significant impact on the values found for the other parameters by the least squares fitting procedure.

Theoretically the spectrum of ^{63}Ni is not expected to have a significant shape factor.[21] Nevertheless, it was found in the analysis that a shape "correction" of the form $S=(1+\alpha E)$ was required in order to obtain a good fit. This is probably caused by uncertainties in the instrumental corrections, e.g., window absorption, penetration through the edges of counter slits, electrostatic effects on transmission, etc. The addition of more terms to the shape correction (e.g., quadratic) made no significant improvement to the fit; it should be noted, however, that the correction for counter window absorption discussed in Sec. V B makes allowance for higher order terms.

B. Fitting procedure

For a given value of m_2 and starting values of the other parameters, a theoretical distribution of the form of Eq. (4) was generated. The response function, $R(p,p')$ (see Sec. C) was folded into the distribution to calculate the number of counts in the channel corresponding to the momentum p.

$$N(p)=\int R(p,p')\frac{dI}{dp'}dp' \ .$$

Standard least squares fitting procedures were then used to optimize simultaneously the parameters K, α, $|U_{e2}|^2$, and E_0. It should be noted that the inclusion of an unknown shape correction (α) does not bias the result obtained for $|U_{e2}|^2$ provided that both parameters are allowed to float simultaneously (as was the case in all results quoted here except where otherwise noted). This reflects the ability of the least squares technique to distinguish between a continuously varying effect in the data and a discontinuous threshold effect. The penalty paid for having an unknown shape correction is that its interdependence with $|U_{e2}|^2$ raises the statistical error of that parameter. All statistical errors quoted in this work include the effects of this correlation.

C. Response function

The main feature of the response function, the optical line shape, was represented by a symmetric Gaussian with full width half maximum $\Delta p/p=0.09\%$ [Fig. 6(a)].

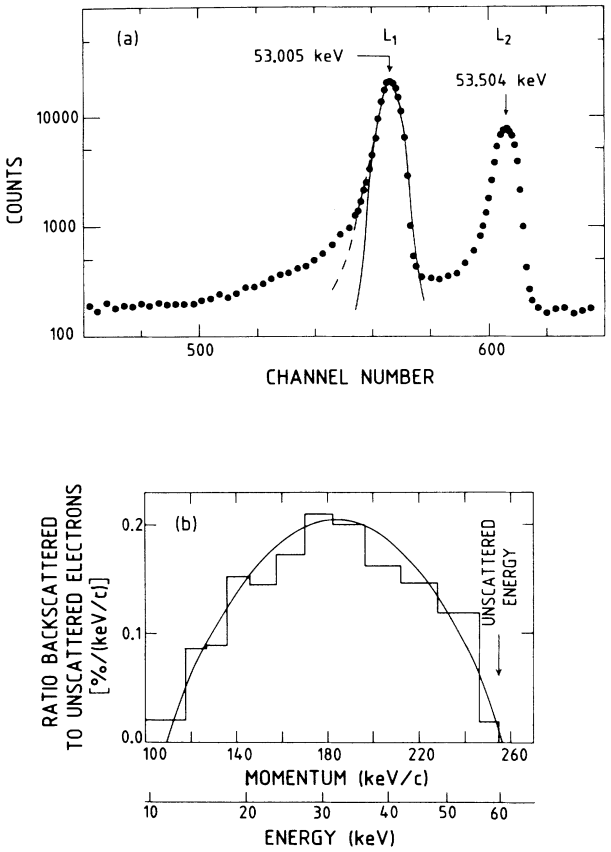

FIG. 6. (a) 53 keV L_1 and L_2 conversion electron lines from ^{169}Yb. The data were collected in 16 counters and consolidated by the same process used for ^{63}Ni. The solid line is the symmetric Gaussian used in the analysis of the beta spectrum. The dashed line includes an exponential tail and was used to test the effects of peak asymmetry on the endpoint energy and other parameters. One channel in the consolidated wide scan ^{63}Ni spectrum corresponds to 25 channels in this spectrum. (b) Calculated momentum distribution for electrons backscattered from the source backing at 20° to the normal. The histogram is a Monte Carlo calculation for a 60 keV mono-energetic point source on the surface of the backing. The total area of the distribution is 18.5% of the intensity of unscattered electrons emitted in the same direction. The fitted parabola was included in the response function used for beta spectrum analysis.

Since the momentum bins of the consolidated spectra were equivalent to either 10 of the narrow-scan or 25 of the wide-scan channels in Fig. 6(a), the exact shape of the peak was not important. The effects on the analysis of a slight asymmetry in the peak was tested by adding an exponential tail on the low energy side [dashed line in Fig. 6(a)]. The long low energy tail in the data of Fig. 6(a) is attributed to shake-up/off effects in the internal conversion process following electron capture[22] and therefore has been assumed not to apply to the beta response function. If some fraction of the shake-up/off

tail is, in fact, present in beta decay, the primary effect will be a small shift in the endpoint energy parameter, E_0; the effect on other parameters is negligible.

In addition to electrons emitted in the forward direction from the source, the data include electrons backscattered from the thick Plexiglas substrate. The momentum distribution for backscattered electrons emerging at 20° to the normal was calculated for various initial energies using a Monte Carlo code (SANDYL).[23] The distribution at all energies was represented in the response function by a parabola [Fig. 6(b)]. The total backscatter fraction, $F_B = 18.5\%$, is independent of energy.

The transmission factor for electrons through the detector window was also included in the response function. The window consisted of two films of polypropylene (average thickness of 55 $\mu g/cm^2$ each) coated in cellulose nitrate, chromium, and gold. The films were mounted in contact with each other to form a single window. The thicknesses of the polypropylene and cellulose nitrate layers were measured to a precision of about $\pm 10\%$ by the color coding method described in Ref. 18. The thicknesses of the metal coatings were measured during evaporation with a quartz crystal thickness monitor. The total average thickness was found to be 168 $\mu g/cm^2$. The transmission of this window at various energies was calculated by the SANDYL code and an analytic function which fits the SANDYL calculations to within $\pm 0.2\%$ was used in the data analysis (see Fig. 7). The effects of nonuniformity in window thickness (up to 20%) and variations in actual electron energy for a given momentum setting (caused by source biasing) were found to be negligible since the change in transmission is nearly linear for small variations of both these parameters. The effect of the uncertainty in the average window thickness was tested by varying the coefficient X in the transmission function. (See Figs. 7 and 9 and Sec. V B.)

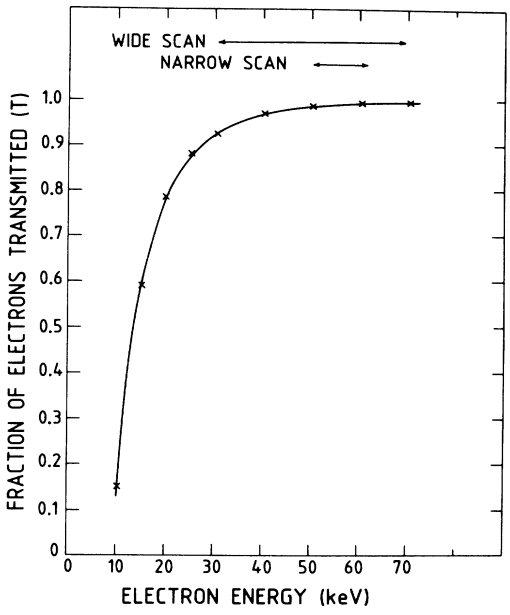

FIG. 7. Detector window transmission showing the Monte Carlo calculations ($\times$) for the 168 $\mu g\,cm^{-2}$ composite window described in the text. The solid line shows the analytic function fitted to the Monte Carlo points that was used in data analysis. It is given by the expression $T = 1 - X \exp[-0.431(E-7)^{0.65}]$, where $X = 2.08$ and E is the kinetic energy in keV. The energy ranges covered by the wide scan data and narrow scan data are shown.

V. RESULTS OF ANALYSIS

A. Endpoint energy

The endpoint energy, E_0, was calculated by a fit to the data from 50 keV to the endpoint to avoid any influence of the hypothesized 17 keV neutrino. The parameters of the best fit are given in the first row of Table I. The endpoint, 66.946±0.010 keV, differs significantly from the value of 65.92±0.15 keV listed in the 1983 Atomic Mass Table.[24]

Estimates of possible systematic errors in the measurement are listed in Table II. The energies of the ^{169}Yb reference lines were calculated from the corresponding gamma energies[25] and the K- and L-shell binding energies.[26] The dominant calibration uncertainty is due to source position. Comparisons were made between several calibration runs during which the ^{63}Ni source was removed and the ^{169}Yb source was installed. The largest measured discrepancy in line energies was 5 eV at 67 keV, i.e., less than that foreseen in Table II. The residual background was varied over the extremes of the range of values compatible with the first 20 channels

TABLE I. Results of the fitting procedure.

Range of data included in fit (keV)	Endpoint E_0 (keV)	Shape coefficient α (keV^{-1})	Mixing fraction $\lvert U_{e2} \rvert^2$	Quality of fit X_ν^2
50–67	66.946±0.010	0.000 56±0.000 16		1.013
26–67	66.941±0.005	0.000 63±0.000 03	−0.0011±0.0010	0.861
26–67	66.946±0.005	0.000 65±0.000 02	0.0[a]	0.862
46–54	66.994±0.123	0.000 30±0.000 27	−0.0017±0.0027	1.142
46–54	66.946[a]	0.000 75±0.000 28	−0.0011±0.0027	1.145

[a]Fixed parameter.

TABLE II. Systematic errors in the measurement of the endpoint of ^{63}Ni.

Cause	Error (eV)
Energy loss in source	5
Response function peak asymmetry	10
Uncertainty in source position (±0.3 mm)	10
Degaussing stability	1
Reference voltage stability	1
Residual background	7

above the endpoint (3±17 counts per channel). Combining all errors (systematic and statistical) in quadrature, we obtain a total error of ±0.020 keV in the endpoint energy.

B. Wide scan spectrum

The consolidated spectrum from the ^{63}Ni wide scan data was analyzed in the region 26–67 keV as described in Sec. IV. The heavy neutrino mass was fixed at 17 keV, and the rest of the parameters were allowed to float; the best fit parameters are shown in the second row of Table I. The endpoint and shape correction coefficients are consistent with those obtained from the data above 50 keV. The value for $|U_{e2}|^2$ is consistent with zero. The negative sign, although physically meaningless, is just as likely to occur in an unconstrained fit as a positive sign, if the true value of the parameter is zero.

The analysis was repeated with the value of $|U_{e2}|^2$ fixed to zero; the best fit parameters (third row of Table I) are consistent with those of the unconstrained fit and there is no apparent systematic trend to the residuals [Fig. 8(a)]. By comparing the two sets of parameters (rows 2 and 3 of Table I), one can see that the mixing fraction is correlated with the endpoint, but the variation is within the statistical error.

The shape correction ($S=1+\alpha E$) is almost certainly not a true shape factor but is necessitated by errors in the instrumental corrections. The magnitude of S increases by about 2.5% from 26 keV to the endpoint at 67 keV. About 0.7% of this can be accounted for if one uses the extrapolated pulse height spectrum to evaluate discriminator losses (Fig. 4). Monte Carlo calculations have shown that another 0.3% is due to penetration at the edges of the detector entrance slit by the higher energy electrons. The remainder could well be accounted for by small uncertainties in backscatter and window transmission, to which this parameter is very sensitive.

In the above fit, the backscatter fraction F_B and the window thickness T were fixed at our best estimate values. In spite of the inclusion of a floating shape correction to account for errors in these parameters, we felt it prudent to assess explicitly the impact of the uncertainties in both corrections on the value of $|U_{e2}|^2$. Varying the parameters individually, it was found that a change in F_B of 5% increased the total χ^2 of the fit by 1 and a change in T of only 1.2% also increased χ^2 by 1. This sensitivity to window thickness is well beyond our

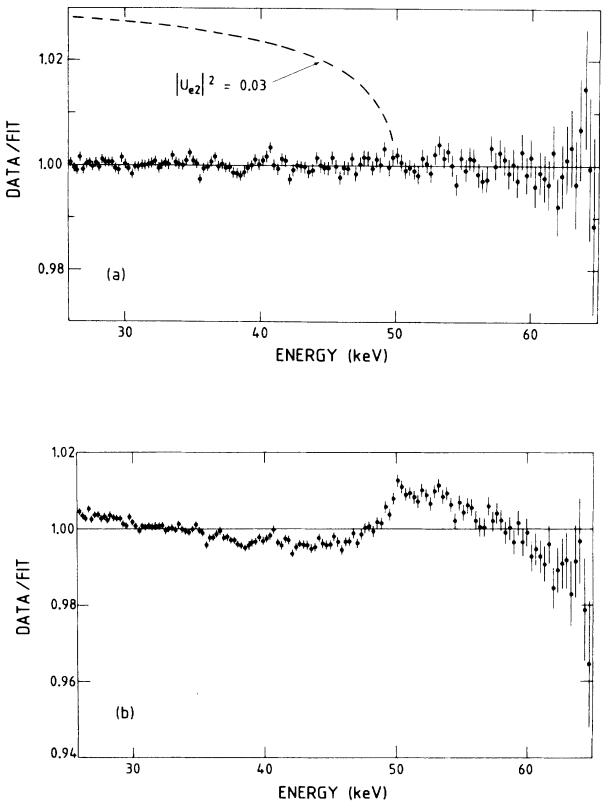

FIG. 8. Ratio of data to fit for the wide scan spectrum. (a) $|U_{e2}|^2$ fixed to zero and the other parameters optimized. For comparison, the dashed line shows the expected shape for $|U_{e2}|^2=3\%$. The best fit parameters are $E_0=66.946$ keV, $\alpha=0.000\,65$ keV^{-1}, and $\chi^2_\nu=0.862$. (b) Best fit for $|U_{e2}|^2$ fixed at 3%. The other parameters optimized are $E_0=67.019$ keV, $\alpha=0.0049$ keV^{-1}, and $\chi^2_\nu=7.76$. The shape of the plot and the reduced χ^2 value clearly rule out this large a mixing fraction for the 17 keV neutrino.

ability to measure this parameter. This means, in effect, that the fit to the ^{63}Ni data itself was the most stringent test available for these corrections and it became necessary to evaluate the uncertainty in $|U_{e2}|^2$ resulting from uncertainty in the two parameters. Assuming that the formulations adopted for backscatter and window transmission have the correct energy dependence, the uncertainty accruing to $|U_{e2}|^2$ from our lack of knowledge of F_B and T was deduced from Fig. 9 to be ±0.0014. This uncertainty, combined in quadrature with that obtained for the fit with F_B and T fixed and $|U_{e2}|^2$ varying (second row of Table I), yields an overall standard deviation of ±0.0017.

For physical reasons, the value of $|U_{e2}|^2$ must be positive. We have no reason to believe that the −0.0011 value obtained from this particular data set is of other than statistical origin. We therefore conclude that the best value for $|U_{e2}|^2$ that can be deduced from this data is zero. The overall standard deviation defines an

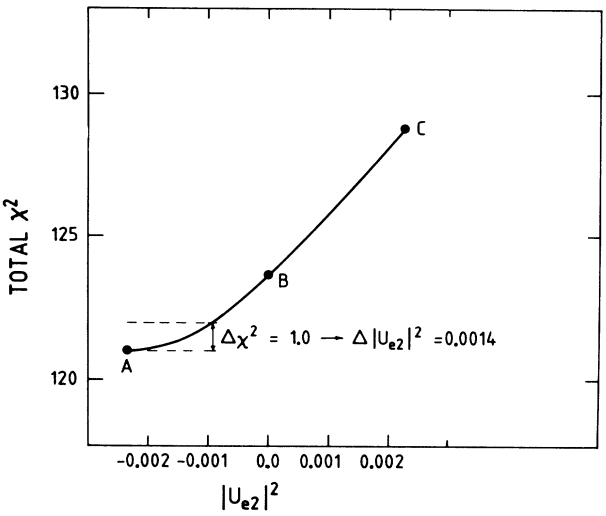

FIG. 9. Variation of total χ^2 with $|U_{e2}|^2$ for 142 degrees of freedom (wide scan spectrum). For each value of $|U_{e2}|^2$, the parameters E_0, α as well as the backscatter fraction, F_B, and window thickness, T, were varied to get the minimum possible value for χ^2. The best fit parameters are as follows:

	A	*B*	*C*
E_0 (keV)	66.945	66.938	66.941
α (keV^{-1})	0.000 50	0.000 72	0.000 84
T (μg cm^{-2})	170	169	167
F_B	0.184	0.192	0.191

One standard deviation for $|U_{e2}|^2$ from this graph (±0.0014) is used as an estimate of the systematic error due to the backscatter and window transmission correction.

upper limit for the mixing fraction of a 17 keV neutrino at (CL denotes confidence limit)

$$|U_{e2}|^2 < 0.0028 \text{ (90\% CL)} .$$

C. Narrow scan spectrum

The narrow scan spectrum was composed of data taken exclusively in the region 46–54 keV plus that portion of the wide scan data in the same region. With all parameters (except the backscatter fraction and window thickness) allowed to float, the best fit for an assumed 17 keV neutrino is obtained with the parameters in the fourth row of Table I. The large error in the endpoint energy reflects the fact that this spectrum does not have data near the endpoint. With the endpoint fixed at our best value (66.946 keV), the best values for the rest of the parameters are those in the fifth row of Table I. The parameters of both fits are consistent with each other and with those of the wide scan fit. It can be seen from the values in the table that, in the narrow scan fits, the endpoint is strongly correlated with the shape coefficient, but its correlation with the mixing fraction is negligible. Similarly, changes in the backscatter and window transmission corrections over a wide range affect the parameter α but have negligible impact on $|U_{e2}|^2$. Consequently, an upper limit for a 17 keV neutrino can be

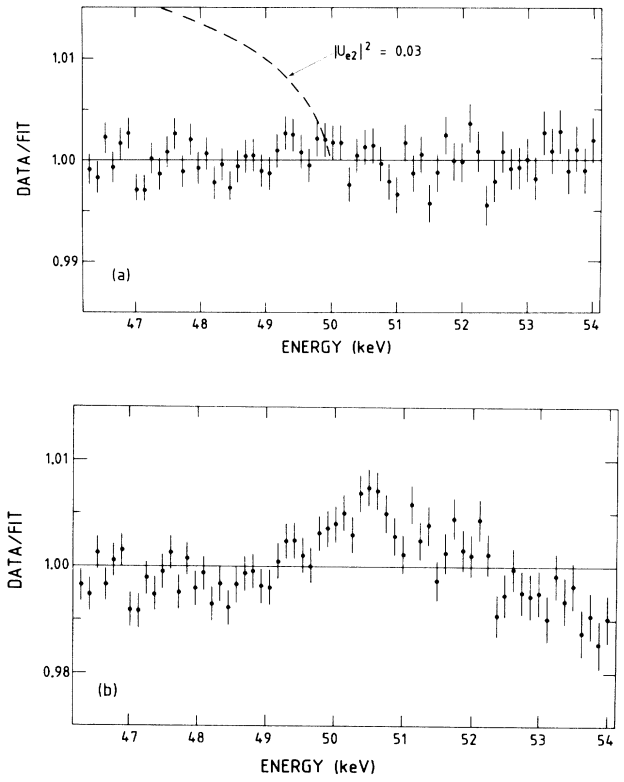

FIG. 10. Ratio of data to fit for the narrow scan spectrum. (a) $|U_{e2}|^2$ fixed to zero, E_0 fixed to 66.946 keV. The dashed curve shows the expected shape for $|U_{e2}|^2=3\%$. The other parameters for the $|U_{e2}|^2=0$ best fit are $\alpha=0.0075$ keV^{-1}, $\chi^2_\nu=1.145$. (b) $|U_{e2}|^2$ fixed to 3%. The other best-fit parameters are $E_0=67.291$ keV, $\alpha=0.0015$ keV^{-1}, $\chi^2_\nu=3.45$. The shape of the plot and the reduced χ^2 clearly rule out a 3% mixing of a 17 keV neutrino.

set from the statistical error alone at

$$|U_{e2}|^2 < 0.0044 \text{ (90\% CL)} .$$

Figure 10(a) shows the ratio of data to the best fit for this spectrum with $|U_{e2}|^2$ set to zero. For comparison, the best fit possible with $|U_{e2}|^2$ fixed at 3% and all other parameters allowed to float is shown in Fig. 10(b).

D. Other heavy neutrino masses

The wide scan spectrum was analyzed for evidence of heavy neutrinos of mass other than 17 keV. For most masses, the best value for $|U_{e2}|^2$ and the upper limit were established in the same way as in Sec. V B. For $m_2 < 10$ keV, only the data from 46 keV to the endpoint were used. In this region the main contribution to the total error is from uncertainty in the endpoint caused by its proximity to the heavy neutrino threshold. The results are summarized in Fig. 11.

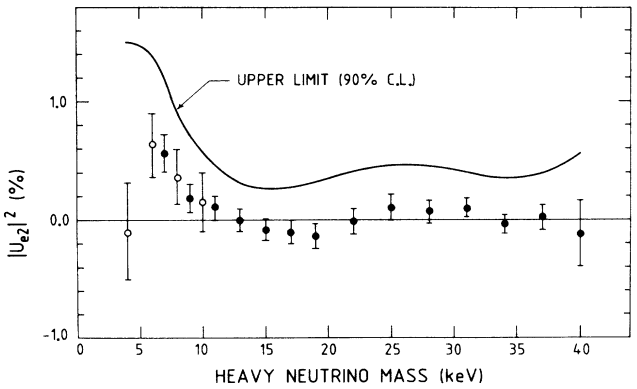

FIG. 11. Mixing fraction for heavy neutrinos with masses in the range 4–40 keV. Each point represents a best fit when E_0, α, and $|U_{e2}|^2$ are allowed to vary. The solid points are fits to all of the wide scan data; the open circles are fits to the data above 46 keV. The error bars represent one standard deviation (statistical). The upper limit line includes an estimate of the systematic error due to the backscatter and window transmission corrections. The slow oscillation in the best fit values may reflect the systematic effect of errors in these corrections.

VI. CONCLUSIONS

We find no evidence in the beta spectrum of ^{63}Ni for the mixture of a heavy neutrino with the usual light neutrino for heavy neutrino masses in the range $4 < m_\nu < 40$ keV. In particular, an upper limit of 0.3% at the 90% confidence level can be set for the mixture of a neutrino with a mass of 17 keV. This is consistent with the upper limit in the range $11 < M_2 < 25$ keV reported by Wark and Boehm[14] and with our earlier data from ^{63}Ni obtained with the Chalk River spectrometer[15] but a thicker detector window. It is also consistent with several measurements,[4–8] of the ^{35}S beta spectrum, but it contradicts the value of 3% reported by Simpson.[1] The stricter limit of $|U_{e2}|^2 < 0.15\%$ given by Ohi *et al.*[5] is probably not warranted on the grounds that other parameters such as E_0 appear to have been fixed to predetermined values in their analysis.[2,9]

It has been argued[2,9] that in order to avoid systematic errors, only a narrow portion of the beta spectrum should be employed in looking for the threshold effect produced by heavy neutrino mixing. If one accepts this argument, our data in the narrow scan region set an upper limit on the mixing of a 17 keV neutrino at 0.44%. However, we feel that concentrating on a narrow region and excluding the rest of the data is not warranted provided adequate care is taken to account for systematic errors. The rest of the spectrum plays an essential role in pinning down other parameters such as the endpoint. Furthermore, concentrating on too narrow a region can lead to the misinterpretation of a local statistical anomaly as a more general trend which, if extrapolated outside the region, would diverge rapidly from the actual data.

We also report a new value for the endpoint of the ^{63}Ni beta spectrum: $E_0 = 66.946 \pm 0.020$ keV. This is more than 1 keV higher than the value $E_0 = 65.92 \pm 0.15$ keV given in the 1983 Atomic Mass Table.[24] From their recent measurement of the ^{63}Ni beta spectrum, Wark and Boehm report an endpoint energy of 65.97 ± 0.12 keV,[14] consistent with the mass table value but significantly lower than the value reported here. In contrast a preliminary analysis of ^{63}Ni data from the iron-free beta spectrometer at the Institute for Nuclear Studies in Tokyo[27] gives an endpoint energy consistent with our value.

ACKNOWLEDGMENTS

The authors are indebted to J. L. Gallant, P. Dmytrenko, and R. H. Martin for preparing the sources used in this research and to L. V. Smith, A. R. Sprake, N. Bray, M. Montaigne, and R. Deal for technical support. Two of us gratefully acknowledge financial support from the Natural Sciences and Engineering Research Council of Canada, D. W. Hetherington for a post doctoral fellowship and R. L. Graham for an operating grant.

*Present address: Physics Department, Vanier College, 821 Ste-Croix Blvd., St. Laurent, Quebec, Canada H4L 3X9.

[1] J. J. Simpson, Phys. Rev. Lett. **54**, 1891 (1985).
[2] J. J. Simpson, in Proceedings of the VIth Moriond Workshop on Massive Neutrinos in Particle Physics and Astrophysics (Tignes, France, 1986).
[3] For example, M. J. Dugan, G. B. Gelmini, H. Georgi, and L. J. Hall, Phys. Rev. Lett. **54**, 2302 (1985); S. L. Glashow and A. Manohar, *ibid.* **54**, 2306 (1985); A. A. Anselm and Z. G. Berezhiani, Phys. Lett. **162B**, 349 (1985).
[4] T. Altzitzoglou *et al.*, Phys. Rev. Lett. **55**, 799 (1985).
[5] T. Ohi *et al.*, Phys. Lett. **160B**, 322 (1985).
[6] A. Apalikov *et al.*, JETP Lett. **42**, 289 (1985).
[7] V. M. Datar *et al.*, Nature (London) **318**, 547 (1985).
[8] J. Markey and F. Boehm, Phys. Rev. C **32**, 2215 (1985).
[9] J. J. Simpson, Phys. Lett. **174B**, 113 (1986).
[10] W. C. Haxton, Phys. Rev. Lett. **55**, 807 (1985).
[11] G. R. Kalbfleisch and K. A. Milton, Phys. Rev. Lett. **55**, 2225 (1985).
[12] B. Eman and D. Tadic, Phys. Rev. C **33**, 2128 (1986).
[13] J. Lindhard and P. G. Hansen, Phys. Rev. Lett. **57**, 965 (1986).
[14] D. Wark and F. Boehm, in *Proceedings of the International Symposium on Nuclear Beta Decays and Neutrinos,* Osaka, Japan (1986), edited by T. Kotani, H. Ejiri, and E. Takasugi (World-Scientific, Singapore, 1986), pp. 391–393.
[15] D. W. Hetherington *et al.*, abstract submitted to and in *Proceedings of the International Symposium on Nuclear Beta Decays and Neutrinos,* Osaka, Japan (1986), edited by T. Kotani, H. Ejiri, and E. Takasugi (World-Scientific, Singapore, 1986), pp. 387–390.
[16] R. L. Graham, G. T. Ewan, and J. S. Geiger, Nucl. Instrum.

Methods **9**, 245 (1960).
[17]R. L. Graham *et al.*, in *Neutrino Mass and Low Energy Weak Interactions* (Telemark, 1984), edited by V. Barger and D. Cline (World-Scientific, Singapore, 1985), pp. 63–69.
[18]D. W. Hetherington, M. A. Lone, and R. L. Graham, Nucl. Instrum. Methods A **242**, 270 (1986).
[19]K. E. Bergkvist, Nucl. Phys. **B39**, 317 (1972).
[20]H. Behrens and J. Janecke, *Numerical Tables for Beta Decay and Electron Capture* (Springer-Verlag, Berlin, 1969).
[21]I. Towner, private communication.
[22]K. E. Bergkvist, Phys. Lett. **154B**, 224 (1985).
[23]H. H. Colbert, SANDYL, a computer program for calculating combined photon-electron transport in complex systems, Sandia Laboratory Report SLL-74-0012, 1974.
[24]A. H. Wapstra and G. Audi, Nucl. Phys. **A432**, 1 (1985).
[25]E. G. Kessler, Jr., L. Jacobs, W. Schwitz, and R. D. Deslattes, Nucl. Instrum. Methods **160**, 435 (1979).
[26]*Table of Isotopes*, 7th ed., edited by C. M. Lederer and V. S. Shirley (Wiley, New York, 1978).
[27]K. Hisatake, private communication.